

# Supplementary Documentation for Reynolds Mountain East FMCW Radar Autopicked Snow Depths, Version 1

Jukes Liu ([jukesliu@boisestate.edu](mailto:jukesliu@boisestate.edu)) and HP Marshall ([hpmarshall@boisestate.edu](mailto:hpmarshall@boisestate.edu))

## I. Data Collection Methods and Acquisition

Radar transects were captured using a 2-10 GHz FMCW radar instrument attached to a pole that was held between two skiers (*Fig. 1*). This radar system is based on a Teledyne YIG oscillator, two directional couplers, and a microwave detector. The system is controlled via a National Instruments (NI) multifunction data acquisition board, with MATLAB acquisition software on a Windows PC laptop. The YIG is sent a voltage signal through NI digital to analog converter (DAC) that creates a linear frequency sweep that is sent to the transmit antenna, and a sample of the transmitted wave is combined with the received wave captured by the receive antenna with directional couplers. The resulting mixed signal is converted to a voltage in the detector, and sampled on the NI analog to digital converter (ADC). This system can perform a full sweep at approximately 20Hz, and data is logged directly to disk on the PC.

The sample design was chosen to measure coincident with the ground validation observations, and locations were determined to sample a range of expected snow depths, vegetation, and to target one of the major drifts in this research watershed. Details of the radar design and processing steps can be found in a review paper (Marshall and Koh, 2008). Data was processed from 2.5-9.5 GHz to avoid artifacts at the end of the frequency range. The antennas used were manufactured by Q-Par and cover a range of 2-18 GHz. The YIG oscillator is rated from 2-10 GHz, the directional couplers from 0.1-10 GHz, and the detector from 0.01-18 GHz. The radar was custom designed and fabricated at Boise State University in collaboration with the U.S. Army Cold Regions Research and Engineering Lab (CRREL).

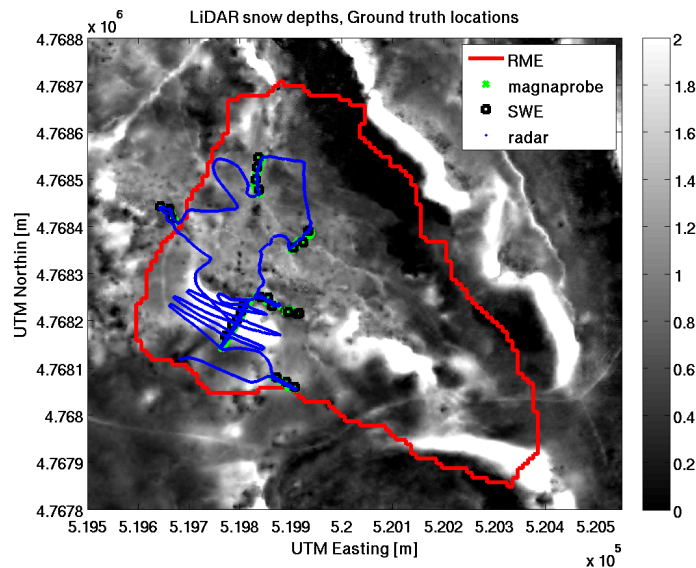


*Fig. 1. Site map with radar lines (blue) for Reynold's Mountain East (RME) over lidar snow depth (in meters). Radar data collected on March 19, 2009, coincident with the lidar snow-on flight and field measurements (magnaprobe, SWE cores).*

## II. Processing Steps

There are several processing steps that are applied to the FMCW radargrams prior to the autopicking of the snow and ground surfaces: 1) sky calibration, 2) removal of flat reflectors, and 3) stitching and splitting into square radargrams. The radar instrument was held upward toward the sky at each site to collect sections of data without any return signal. The sky calibration sections are then subtracted from all the radargrams to remove instrument noise (Fig. 2). After the sky calibration, some flat reflectors corresponding to instrument noise may still remain. The rows of each radargram that all contain the same value within a 2 sigma noise threshold are removed (Fig. 2). To further eliminate the flat reflectors occurring below the ground reflection, we vertically subset all the radargrams at a standard depth, just below where ground reflections are visible. The final radargrams are then all stitched together and re-split horizontally into square images because square images process faster through the wavelet-based autopicking algorithm, described below.

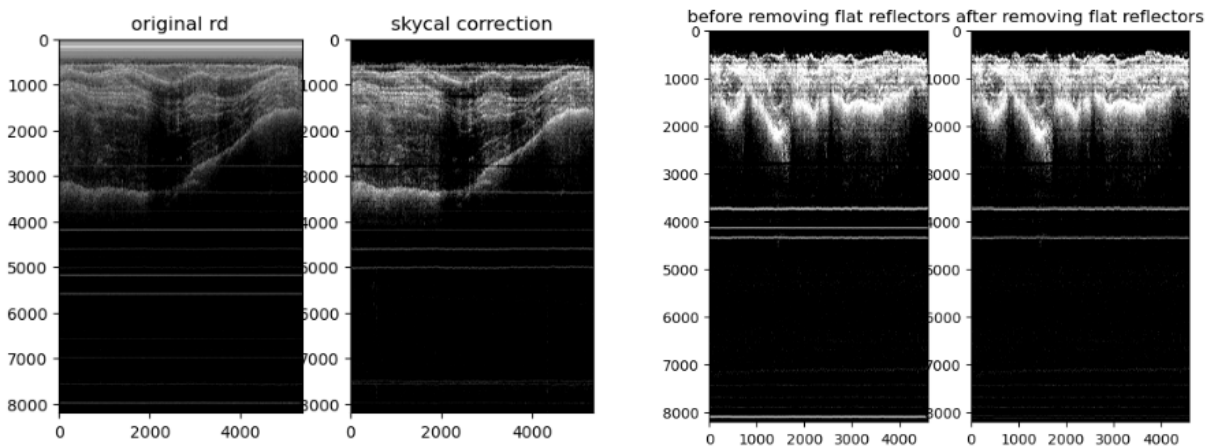


*Fig. 2. Original radargram (rd) section from Reynold's Mountain East and the pre-processing corrections: the sky calibration and removal of flat reflectors.*

We then apply the 2D Wavelet Transform Modulus Maxima (WTMM) segmentation method to the radargrams, which produces contour lines along interfaces of high brightness change throughout each radar image. The 2D WTMM segmentation method has been used to identify regions of high brightness change in optical satellite images (Liu et al., 2021), biomedical imagery (Khalil et al., 2007), and more (McAteer et al., 2010). The open-source python implementation of the 2D WTMM segmentation method is available as a part of a GitHub repository containing code that applies it to trace glacier terminus positions in Landsat images (<https://github.com/jukesliu/automated-glacier-terminus>; Liu & Kinzelman, 2024). Adjustable parameters include the spatial scale of the applied wavelet transform, the minimum length (i.e., size) of the resulting delineations, and a minimum mean brightness gradient (i.e., mean modulus) value.

We applied the 2D WTMM at a range of spatial scales (400-1500 pixels) and determined the optimal wavelet scale of 1000 pixels for producing continuous delineations along the surface

and ground interfaces. Only the delineations that contain mean brightness gradient values above the mean value of all the delineations in the radargram and that are longer than 100 pixels were kept. Out of the remaining delineations, the snow surface and snow-ground interfaces are picked for each trace. The snow surface pick is the first point at which there is a delineation that passes the mean brightness gradient and length threshold, below a threshold in y-index (e.g., 700 pixels from the top of the image in Fig. X below) to eliminate traces of instrument noise above the snow surface that were not removed during the sky calibration. The ground pick is the last point at which there is a delineation that passes the mean brightness gradient and length threshold. The resulting ground pick typically corresponded to the bottom edge of the ground reflection, whereas the location of the ground interface should correspond to the peak brightness in the ground reflection (Fig. 3). To address this offset, we apply a linear shift to the ground pick based on comparison with a lidar snow depth map.

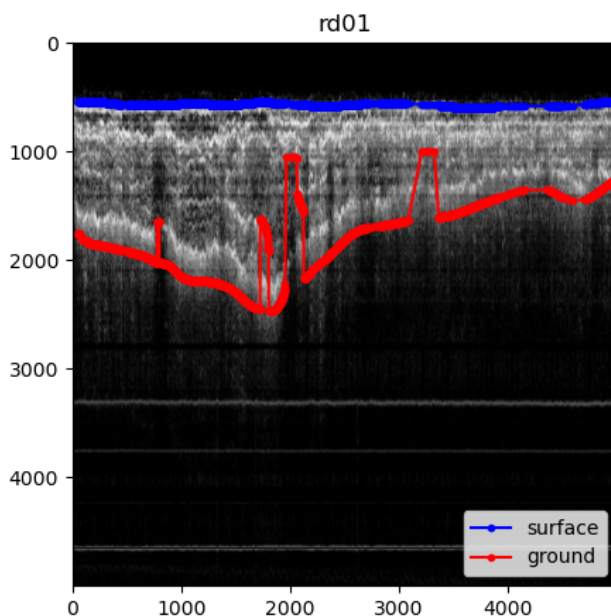


*Fig. 3. Autopicked snow and ground surface reflections in a radargram section from Reynold's Mountain East.*

Subsequent manual cleaning and shifting of the radar picks requires a coincident snow depth map from a snow-on and snow-off lidar flight. For Reynold's Mountain, we used the lidar depth map from a snow-off flight from November 10-18, 2007 and a snow-on flight from March 19, 2009 (Shrestha, 2016). Lidar snow depths that coincide spatially with the radar transects are extracted using the x,y coordinates of each radar trace. The resulting 1 to 1 plot of the lidar and radar snow depths indicate that a slope of 1 is appropriate, however, the best-fit intercept of the line is nonzero, indicating the radar depths are systematically offset from the lidar depths. As discussed above, the systematic offset can be attributed to the WTMM pick of the lower edge of the ground reflection. We use a python widget to manually shift the intercept of the 1 to 1 line to produce the highest correlation value and lowest RMSE between the radar and lidar depths (Fig. 4a). The shifted depths are then displayed over each radargram section in the lasso

selector widget. The user visually inspects the ground picks and can use the lasso tool to remove inaccurate picks (Fig. 4b). This step may be repeated multiple times if necessary.

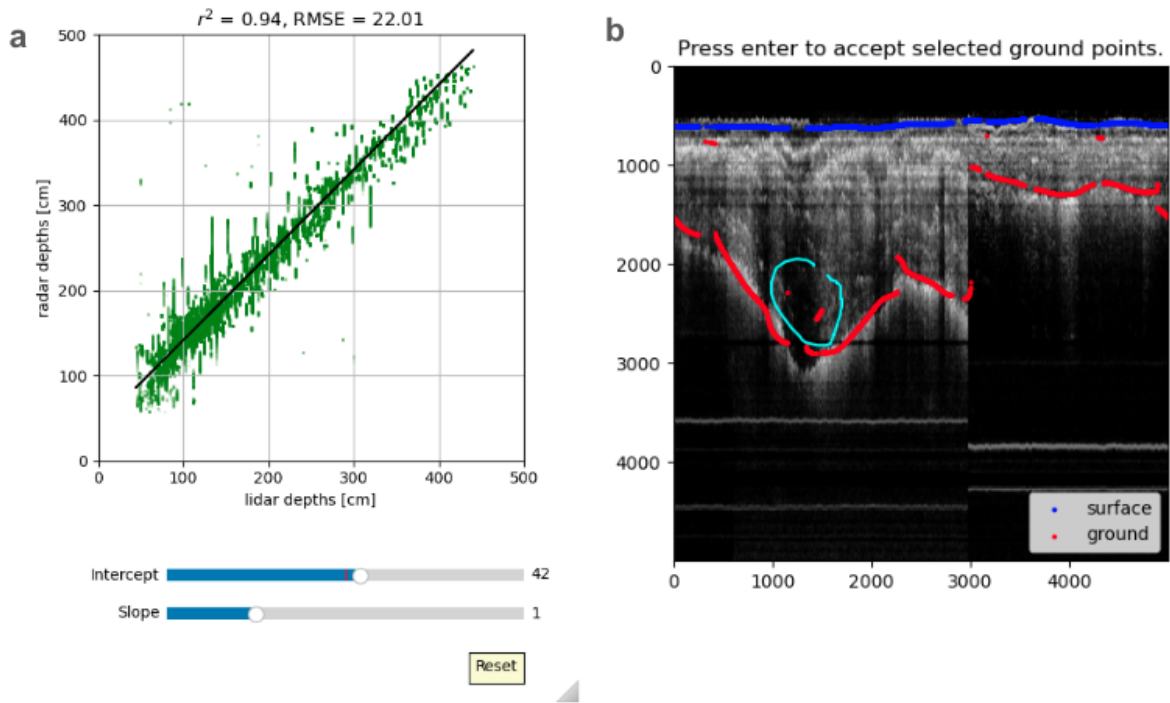


Fig. 4. Python widgets used to manually filter and adjust the WTMM radar depths. a) 1 to 1 radar vs. lidar depth intercept shift. b) Lasso selection to remove incorrect ground picks.

The final results with the linear shift align well with the snow depths from the lidar depth map (Fig. 5). The uncertainties, errors, and limitations are addressed in the following section. Code to process the FMCW radar outputs are contained in a GitHub repository:

<https://github.com/jukesliu/snow-radar>.

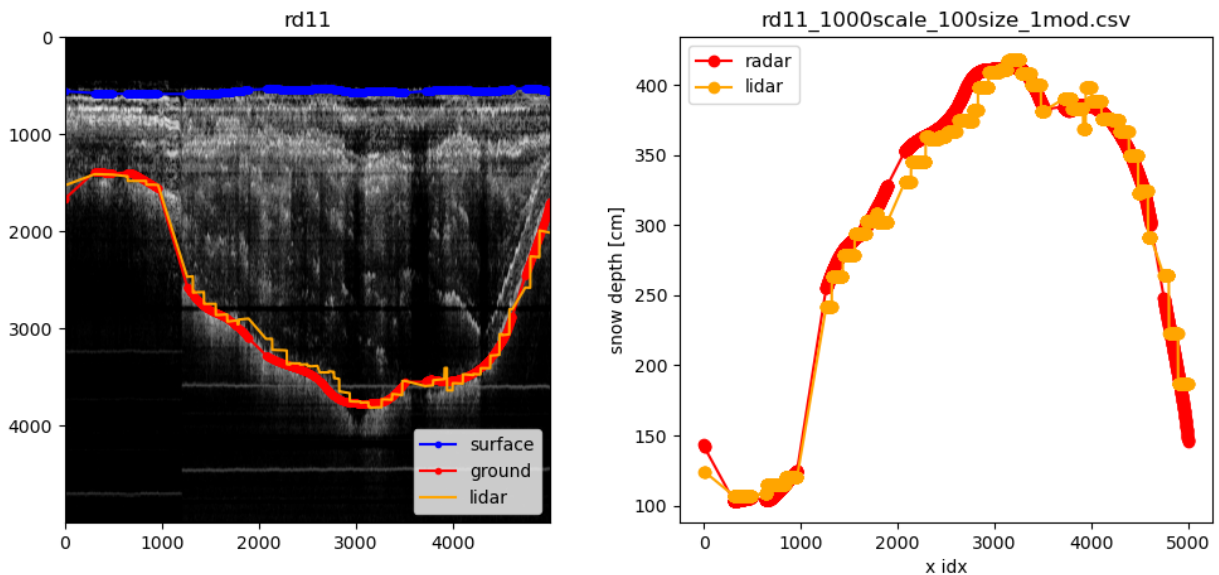


Fig. 5. Shifted radar ground surface autopicks align closely with the lidar snow depth map.

### III. Errors and Uncertainties

We assessed the error of the FMCW radar autopicked snow depths through comparison with the overlapping lidar and probe measurements across a ~4-meter deep snow drift at Reynolds Mountain East. This location was chosen due to the overlap of the three datasets and the range of snow depths represented throughout the ~100-meter wide snow drift. Comparison of the lidar depth and radar ground picks along the snow drift indicate that the spatial patterns in snow depth from the two data sources match closely (Fig. 6). The probe, lidar, and radar depths along the drift were spatially-averaged using a moving 3-meter window (Fig. 7), equal to the ~3-meter GPS uncertainty for all instruments.

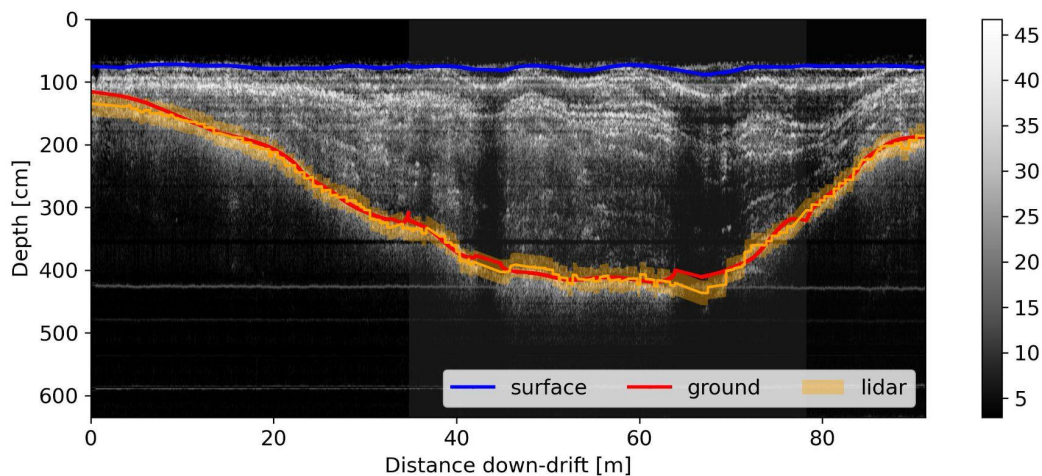


Fig. 6. Snow depths across a snow drift in Reynolds Mountain East from the radar surface and

ground picks over the radargram and the lidar depth map (orange) with 20 cm depth uncertainty.

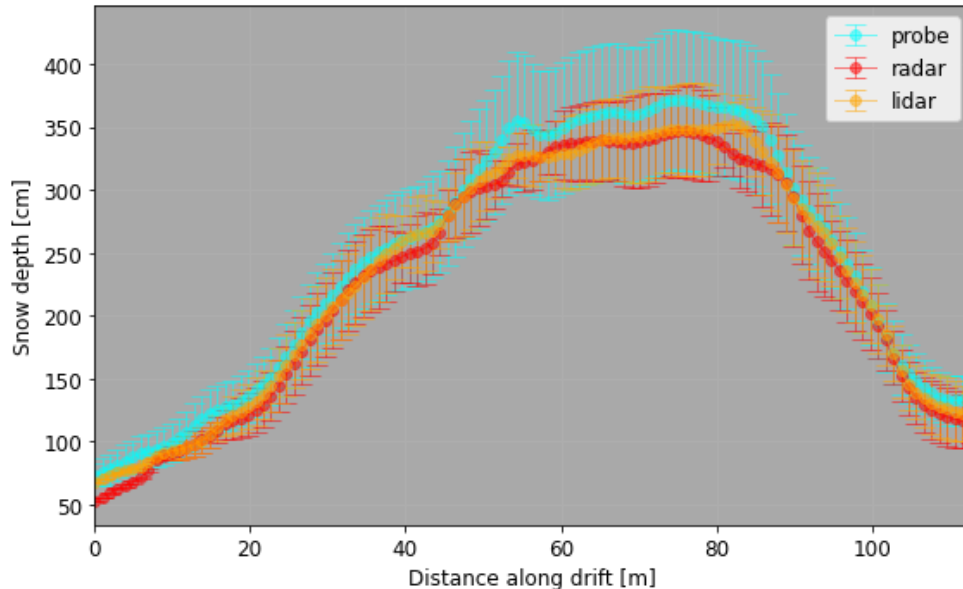


Fig. 7. Comparison of snow depth in the drift. Weighted average snow depth calculated within a 3-meter window. Error bars correspond to the standard deviation in the weighted values.

The profiles of snow depth in the drift indicate that the radar and lidar depths match closely with an RMSE of 5 cm, ~2% of the mean snow depth (Fig. 8). Only the shallowest snow depths deviate. The radar picks appear to underestimate snow depth in the first 10 meters along the drift (Fig. 7 & 8). Meanwhile, the radar and probe depths have a higher RMSE of 17 cm, ~8% of the mean snow depth. The 1 to 1 plot shows a systematic offset between the radar and probe depths (Fig. 8). Radar and lidar depths were consistently shallower than the probe measurements, possibly due to overprobing, a common error in manual measurement of snow depths. Furthermore, the radar and lidar estimates are likely influenced by woody shrub just above the ground interface whereas manual probing is able to puncture through the shrub layer. Overall, the uncertainty analysis in the drift indicates that the radar snow depth uncertainties are 5-18 cm across a wide depth range of 0 to 400 cm.

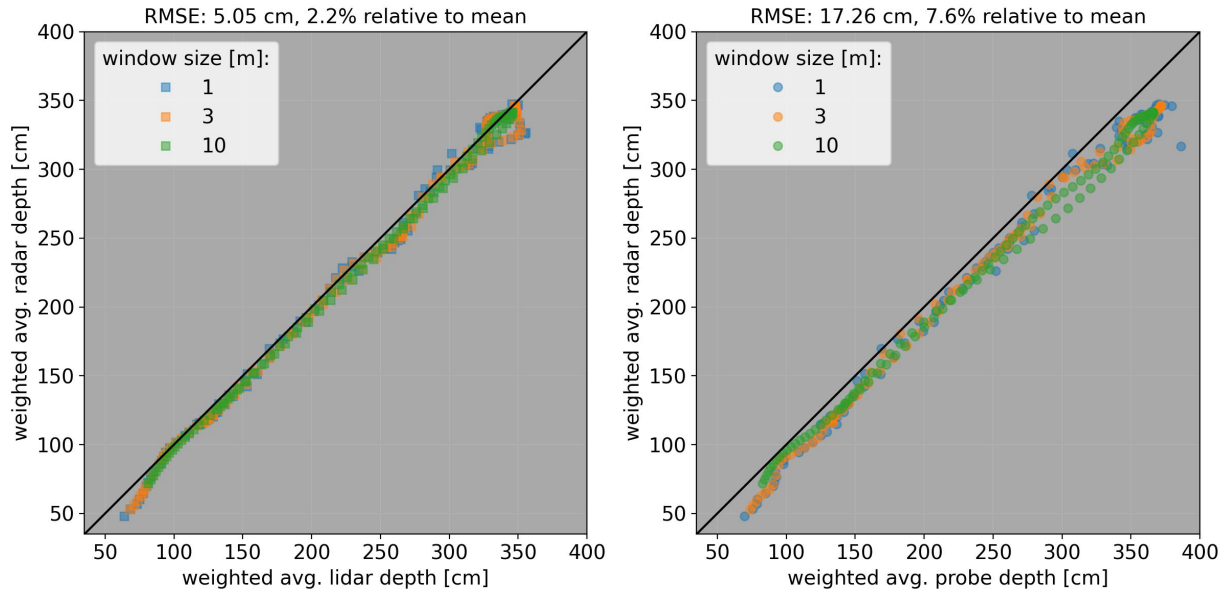


Fig. 8. Comparison of the data in the snow drift in 1-to-1 plots with different averaging window sizes (1, 3, and 10 meters).

## References

- Khalil, A., Grant, J. L., Caddle, L. B., Atzema, E., Mills, K. D., and Arneodo, A. (2007). Chromosome territories have a highly nonspherical morphology and nonrandom positioning," *Chromosome Res.*, vol. 15, no. 7, pp. 899–916.
- Liu, J., Enderlin, E. M., Marshall, H. P., and Khalil, A. (2021). Automated Detection of Marine Glacier Calving Fronts Using the 2-D Wavelet Transform Modulus Maxima Segmentation Method. *IEEE Transactions on Geoscience and Remote Sensing*, vol. 59, no. 11, pp. 9047-9056. doi: 10.1109/TGRS.2021.3053235
- Liu, J. & Kinezelman, P. (2024). automated-glacier-terminus: v 1.1.2. [software]. Published at <https://doi.org/10.5281/zenodo.5898573>
- McAteer, R. T. J., Kestener, P., Arneodo, A., and Khalil, A. (2010). Automated detection of coronal loops using a wavelet transform modulus maxima method," *Sol. Phys.*, vol. 262, no. 2, pp. 387–397.
- Shrestha, Rupesh. (2016). *2009 1m Snow Depth for Reynolds Mountain East, Reynolds Creek Experimental Watershed, Idaho* [Data set]. Retrieved from <http://doi.org/10.18122/B28597>